ISSN 2070-2051, Protection of Metals and Physical Chemistry of Surfaces, 2020, Vol. 56, No. 5, pp. 998–1007. © Pleiades Publishing, Ltd., 2020.

NEW SUBSTANCES, MATERIALS, AND COATINGS

Microstructural and Mechanical Behaviour of WC Reinforced Particles A3003 Surface Composite Fabricated through Friction Stir Processing

Surendra Kumar Patel[a, *], Raman Nateriya[b], Barnik Saha Roy[c], and Basil Kuriachen[a]

[a] *Department of Mechanical Engineering, National Institute of Technology Mizoram, Aizawl, 796012 India*
[b] *Department of Civil Engineering, Maulana Azad National Institute of Technology, Bhopal, 462003 India*
[c] *Department of Mechanical Engineering, National Institute of Technology Agartala, Tripura, 799046 India*
**e-mail: surendrakumarptl@gmail.com*

Received January 16, 2020; revised April 19, 2020; accepted April 24, 2020

Abstract—In this current research, tungsten carbide (WC) micro-particles were dispersed into an aluminium (A3003) matrix by the way of multi-pass friction stir process (FSP) to fabricate a new surface composite (hereafter referred to as WC/A3003). Mechanical and microstructure properties affected by the influence number of stirred passes (FSP passes) were studied in detail. The microstructural studies showed that increasing the number of processed passes provided to the uniform dispersion and improved grain-refinement of WC micro-particles. The microstructural examination of the interface indicated excellent intermetallic metallurgical grains bonding between the matrix and the solid solution of WC/A3003 matrix. The mechanical outcomes showed that microhardness improved with a more homogenous spreading of reinforcement by increasing the FSP passes. The strength and ductility of the processed composites were also enhanced. As a result, a tensile strength, microhardness, and ductility of 143 MPa, 91.5 HV, and 30% elongation, respectively, were achieved in the 6-pass composite. Thus, the detailed studies of the as-developed composites provided many interesting and useful outcomes for further siding and roofing applications.

Keywords: A3003 alloy, tungsten carbide, surface composite, FE-SEM, friction stir processing
DOI: 10.1134/S2070205120050226

1. INTRODUCTION

Aluminium-based hybrid metal matrix composites (AHMMCs) with incorporation of reinforcement particles are progressively used in the automotive, aerospace, marine and structural industries such as; pressure vessel, gasoline tanks, garage doors, storage tanks etc due to their high specific strength, low density, high stiffness as well as better thermal stability and good wear resistance [1–3]. Generally, ceramic or carbide particles (ZrO_2, SiC, Al_2O_3, TiC, B_4C, etc.) enhance the strength, wear resistance, and elastic modulus of the matrix, which are disengaged with the reinforcements. However, the strength introduced by the carbide particles is inversely proportional to the ductility because of the de-bonding of the particulate hybrid metal matrix and the development of porosity at the ceramic-matrix interface. Typically, it is caused by the better wettability and high incompatibility between the thermal coefficient of the development of metal matrix composite with incorporation of reinforcement particles [4]. The secondary particles and brittle interface formed by biochemical reactions during the joining process encourage easy nucleation and dissemination during plastic deformation [5, 6]. Furthermore, carbide- or ceramic-reinforced aluminium metal matrix composite grieve decrease in electrical resistivity because of the reduced electrical resistivity of the carbide or ceramic particles [7]. The electrical resistivity of AMCs used as rocket or aerospace constituents must be measured because the development of static electricity in the spacecraft has damaging consequences on the safety of shuttle flights. These disadvantages significantly limit the widespread application of the composites. Consequently, there is an urgent need for the development of new types of reinforcement particles [8]. Firm metallic units have been employed as additional support for carbide particles in composites because of their good wettability and coefficient of thermal expansion being closer to Al-metal matrix, which might endow a better amalgamation of strength, ductility and intermetallic bonding to the matrix [9, 10].

The metal particle-reinforced Al-metal-matrix composites (AMMCs) may reveal excellent mechanical, thermal, and electrical properties if no intermetallic bonding occurs at the developed matrix interface [11]. Regrettably, so far comparatively very little con-

Table 1. Elemental composition of aluminium alloy (A3003)

Material	Mn	Fe	Si	Cu	Zr	Al
Wt %	1.2	0.7	0.60	0.1	0.1	Balance

sideration has been paid to new classifications of reinforcing carbide particles so far because of the low reactivity of aluminum alloys. Moreover, the development of a brittle intermetallic interface causes premature rupture by smoothing cracks [12]. The traditional melting processes such as stir-casting are not suitable to join carbide particulates reinforced (MPR) because of the high fabricating temperature [13]. Accordingly, proposed a procedure called fragmented metal deposition (FMD) for producing AMMCs reinforced with TiC, W, SiC, Ni, or B_4C particles. FMD involves several complex steps: pre-heat behaviour of melting Al-reinforcement mixture emotive the heat zone, metal stirring action, and decomposition of the melt to end formation. However, the heat treatment of titanium or nickel nanoparticles may reduce the interface into aluminium and titanium-based composites [14]. Therefore, an opportunity for the development of brittle intermetallic interfaces between aluminium and reinforcement particles, which cannot be left out. The fabricated particles reveal large number of thin micro and nano layers into Al–Ti intermetallic near un-reacted titanium grains, so that cracks formations generated during the solidification. It is very difficult to circumvent formed intermetallic layer during the exploration process, which is a relatively high temperature process (HTP) [15]. To developed the FSP surface as a simple and cost-effective solid-state metal joining technique basically based on the several plastic deformations, modification as well as grain refinement of the particles and microstructure [16]. The procedure has been fundamentally developed for the microstructural alteration of constituents (metal with or without reinforcement) and can also be used to produce surface composites through the development of grooves [17] and groove-filling phenomenon after introducing reinforcement particles into the materials [18].

Many researchers suggested that friction stir processing might cause effective severe plastic deformation (fraternisation) of the material into processed area, where the strain-index could be higher. Thus, reinforcement particles could be introduced into the processed zone of the composites [19]. The severe plastic deformation (fraternization) by solid-state dispensation technique, FSP has higher potential for controlling the particles dynamic-kinetics of interfacial zone into the matrix and the ceramic/carbide reinforcement particles hindering the reaction in the matrix and reinforcement particles [20, 21]. The studies of surface fabricated composites by FSP have been focused on carbide as reinforcement particles [22]. Also, the investigators have reported high tensile strength and ductility in metal-reinforced AHMMCs due to excellent reinforcement bonding into the developed matrix without the formation of detrimental interfacial phase between the reinforcement and the matrix [23]. The metal particulate-reinforced AHMMCs can be fabricated by FSP. Tungsten carbide (WC) possesses extraordinary properties, like high stiffness, high melting point, better strength, excellent chemical reaction, and superior erosion-corrosion resistance [24]. Specially, tungsten carbide particles exhibit improved electrical-resistivity than ceramic particles [25].

Therefore, in the present investigation, WC particles were employed as reinforcement into an aluminium alloy (A3003), and the resulting composite was fabricated through FSP. However, not much studies have been examined by the effects of multiple passes FSP (2, 4, and 6 passes) among the mechanical, microstructure and tribological properties (e.g. tensile strength, microhardness and erosion-corrosion) of processed surface composites reinforced with tungsten carbide particles.

2. MATERIALS AND METHODS

Commercially, available uncontaminated sheets of the aluminum alloy (A3003) were cut into rectangles 180 mm long, 120 mm wide, and 6 mm thick, as revealed in Fig. 1a. The elemental composition of A3003 is revealed in Table-1. Commercially available, analytical grade WC reinforcement powder (purity = 99.9%) shown in Fig. 2 was used in this study.

To introduce the WC particles into the aluminum alloy (A3003), grooves of the same depth and a width of 3 mm were carved. The grooves ended along the longitudinal path of the alloying plate, in which the WC particles were placed and crushed. The aluminium sheet and pre-placed WC particles were fixed on a supporting aluminum plate for the duration of FSP. To escape the putout of reinforcement particles at time of FSP, the grooves were covered with a smooth conical flat shoulder. The processing was carried out using a numerically-controlled milling machine through the friction stir processing tool of the WC, by a shoulder diameter of 20 mm, conical unthreaded pin root diameter of 8 mm, tip diameter of 6 mm, length of 5 mm and tilt angle of 0°. For development defect-free surface, the tool rotation speed and the linear speed were set as 800 rpm and 40 mm/min, respectively.

The pin was moved along the same line in the different passes during FSP. After each pass, the work pieces were cooled at room temperature before the next pass. The fabrication of the surface composite is schematically summarised in Fig. 3. The shape and grooves were varied to obtain an adequate volume of reinforcement particles in the processed zone. Herein, the theoretical volume fraction of WC powder in the groove was calculated with the following expression to be about 36 vol % [26]:

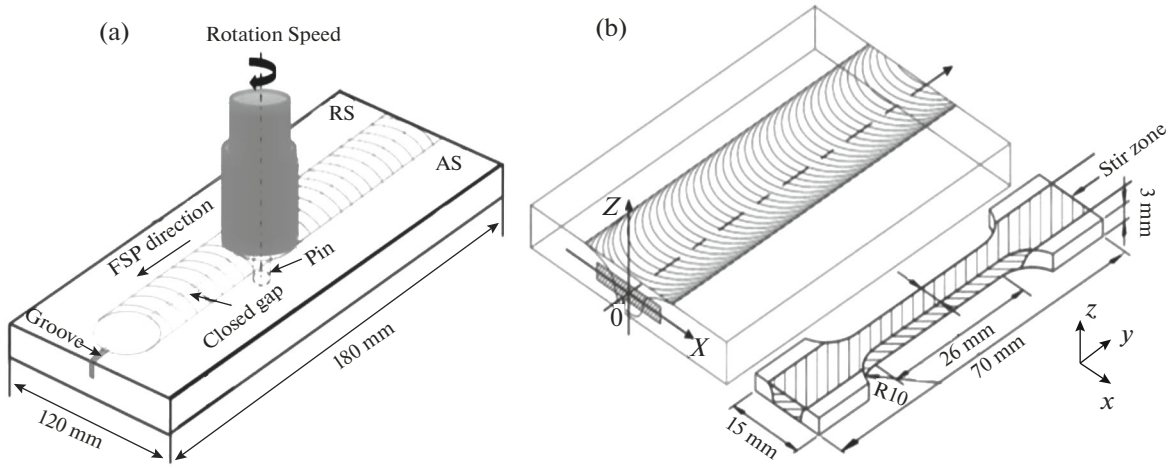

Fig. 1. Schematic drawing of (a) the process of FSP in stir zone and (b) tensile testing sample.

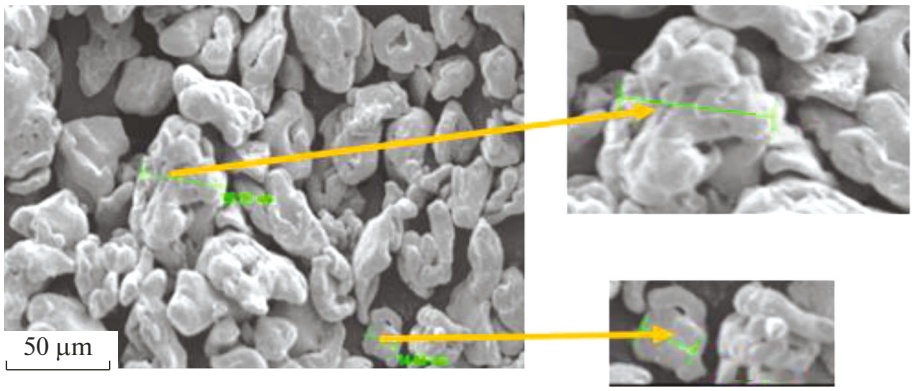

Fig. 2. FE-SEM image of micro tungsten carbide powder.

$$V_t = \frac{A_g}{A_t} \times 100\ \%, \quad (1)$$

where V_t is the theoretical volume ratio, A_g is the area of the groove, and A_t is the area of the tool pin.

The fabricated surface at different FSP-passes were observed by field emission scanning electron microscopy (FE-SEM), and energy dispersive X-ray microanalysis. The measurement of the grain size of the base metal and processed zone (with or without FSP) was carried out by the linear intercept method with properly polished and etched with Keller's reagent. The governing phases, which showed that a WC particle-reinforced surface composite was achieved, were observed by X-ray diffraction (XRD).

The tensile samples were prepared consistent with the ASTM norms (E8/E8M-11) to the necessary dimensions. The sample dimensions are revealed in Fig. 1b. Microhardness observation were made along the cross-section of the hunk (nugget) area of processed samples (10 × 5 × 3 mm) with an HMV-G21 tester with a 200 g load for 20 s.

3. RESULTS AND DISCUSSION

The preliminary analysis of the microstructure and chemical description suggests to enhances the FSP and classify reaction products by the side of WC/A3003 boundaries (interface). The mechanical properties (tensile strength, microhardness) and the fracture surface analysis of the processed surface composites with different numbers of passes are summarised in details in Fig. 3. The effect of different FSP passes among microstructural and enhanced mechanical properties of the processed surface reinforced with WC micro particles is discussed.

3.1. X-ray Diffraction Analysis

XRD analysis was employed to determine the presence of current stages in the 6-pass processed surface

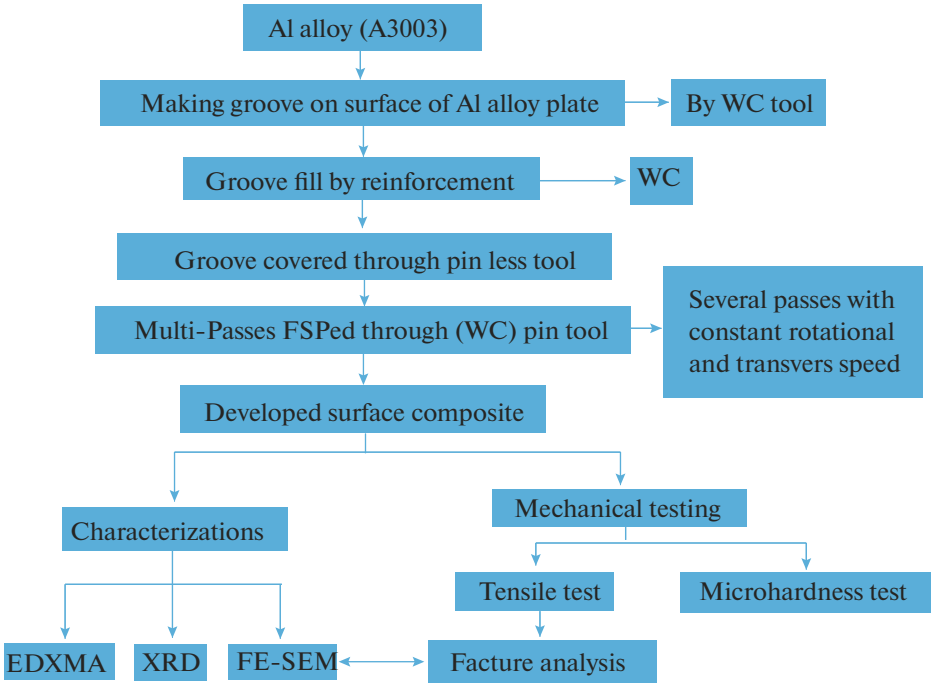

Fig. 3. Schematic synthesis processes of A3003 alloy composites through FSP technique.

composite, and the spectra are shown in Fig. 4. The peaks of tungsten carbide (WC) and A3003 are evidently observed, while no peaks of the WC/A3003 intermetallic and tungsten oxides are present. The absence of a matrix interface and tungsten oxides is accredited to the comparatively low (450°) processing temperature. Moreover, an intermetallic and tungsten oxides are not formed during the 2 and 4-pass processing for of the smaller thermal exposure and heat input. It was testified that the maximum (650°) temperature of the processed zone of various aluminum alloys during FSP was varying with 0.5 to 0.8 T_m [27], corresponding to 0.14–0.21 T_m for WC, which was stimulate to diffusion bonding of WC particles into the matrix.

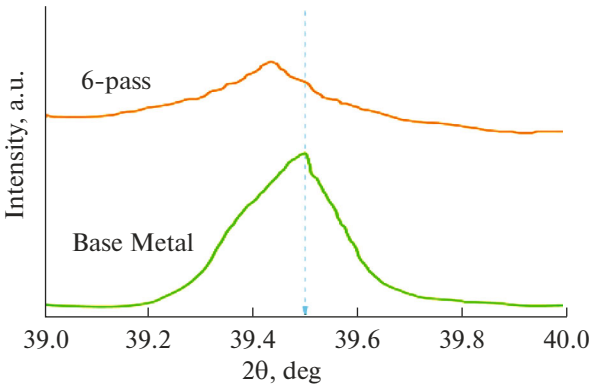

Fig. 4. XRD spectrum of base metal and 6-pass composite view of Bragg angle between ($39° \le 2\theta \le 40°$).

In adding, X-ray diffraction cannot be applied to detect phases present at a low concentration.

3.2. Microstructural Analysis

The FE-SEM micro images (properly polished and etched with suitable etchant) of the processed surface composites fabricated with different numbers of passes are shown in Figs. 5a–5c. Figure 5a shows the presence of WC clusters after 2 passes, and a smaller volume of A3003 is occupied with clusters of tungsten carbide particles. There are two causes for this behaviour: first, when the WC particles fill the developed groove, the pressure (WC powder) brings the contact surface and cold joint together. Secondly, a large residual strain index and stress of the aluminium alloy plate is formed owing to the softening of the material, which is caused by the poor plastic flow during FSP on acquired aluminium and aluminum alloys. The particle size of the tungsten carbide clusters decreases significantly with increase the number FSP passes. As exposed in Fig. 5b, less amount of WC particles are clusters as detected over the 4-pass FSP processed surface, whereas a much more uniform distribution of WC particles are observed after 6-pass FSP surface composite compared to the 2- and 4-pass samples, as seen in Fig. 5c.

This uniformity is attributed to the accumulation of plastic strain and repeated thermal effect, plastic distortion, and mixing in the stir zone. However, did not observe changes in the grain size of the reinforcement particles after increasing the number of FSP passes

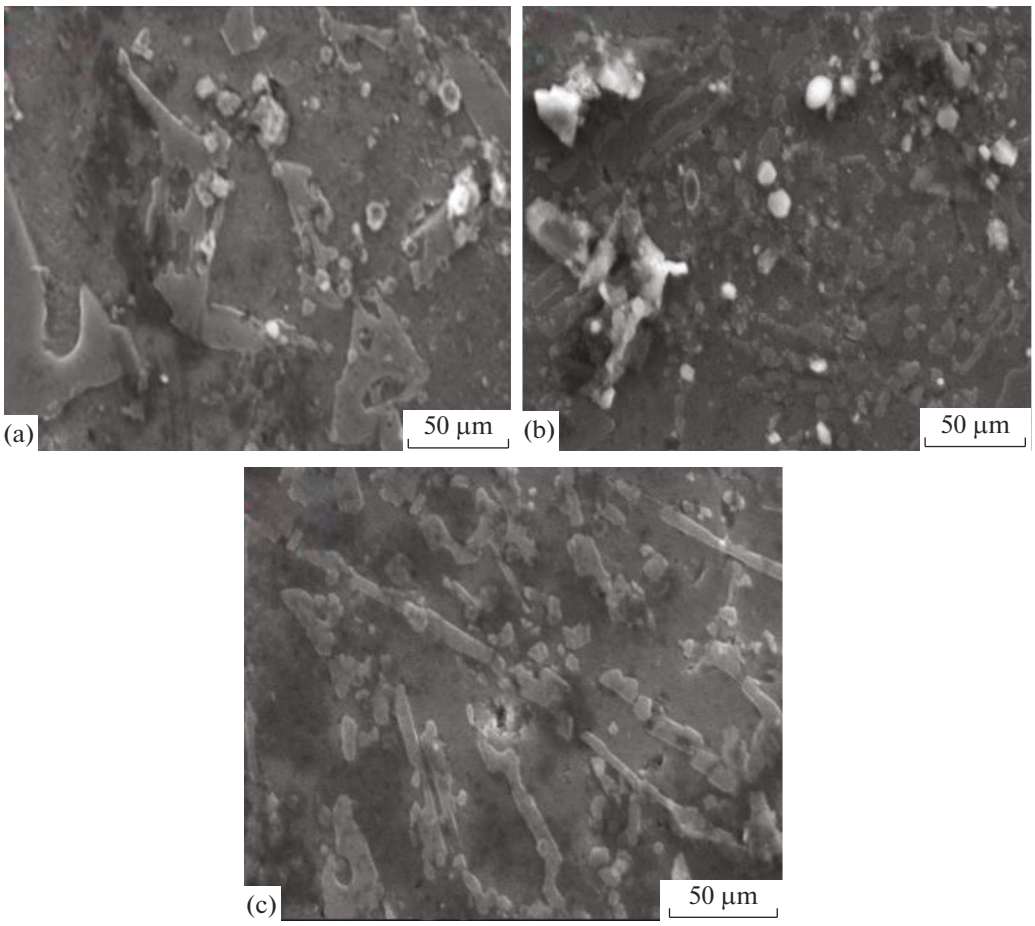

Fig. 5. FE-SEM images of FSP composite (a) 2-pass; (b) 4-pass and (c) 6-pass.

[28]. Moreover, showed that the ceramic particle size and morphology may change during energetic stirring, and several plastic strains may cause fracture, which is related to the smaller size of the WC powder particles [29]. Therefore, the FE-SEM micrographs of the fabricated composites reveal the absence of WC particles during all the steps of polishing, and a WC/A3003 interface was effectively developed. Moreover, the uniformity of the microstructure after 6 passes confirms the effectiveness of the FSP. The grain boundary between the WC/A3003 particles matrix on higher magnification is revealed in Fig. 7.

The WC/A3003 interface shows excellent interfacial integrity as no micropores are observed because the plastically stretched A3003 melts the entire stirred surface of the WC particles. As a result, micro holes and contact bonding does not occur at the WC/A3003 interface. Furthermore, the FE-SEM images of the 6-pass processed surface composites show bright matrix (stir zone) interfaces and no noticeable formation of coating. A high interfacial performance is achieved due to the absence of brittle components in the matrix, thus improving the strength and ductility of the fabricated surface composites.

To govern the dispersion of adjacent particles (WC/A3003) at the interface, the matrix examination and map scanning of the contact zone of the 6-pass FSP WC/A3003 composite were carried out. Figure 6 shows the crossing point of the FE-SEM image and the equivalent line scan detection of the EDXMA analysis of the WC/A3003 surface composite. The EDXMA results in Fig. 6b correspond to the red arrow across the WC particle in Fig. 6a and show the occurrence of a dispersion layer at the WC/A3003 interface containing a solidus solution instead of a matrix intermetallic.

The interface distribution layer consists of a solid solution metallurgically bonded to the tungsten carbide/A3003 interfacial line, which successfully tolerates the load to transmission from stronger WC particles through plastically distortion into matrix. Hence, superior strength and better ductility may arise in FSP matrix. As per interface structural analysis, better solubility of WC into A3003 may occur in the examined temperature range of FSP. It was suggested that Hume–Rothery guidelines state that for excellent solubility two different metals at sensible heat, the metallic ranges of the materials fluctuate up to 17% and

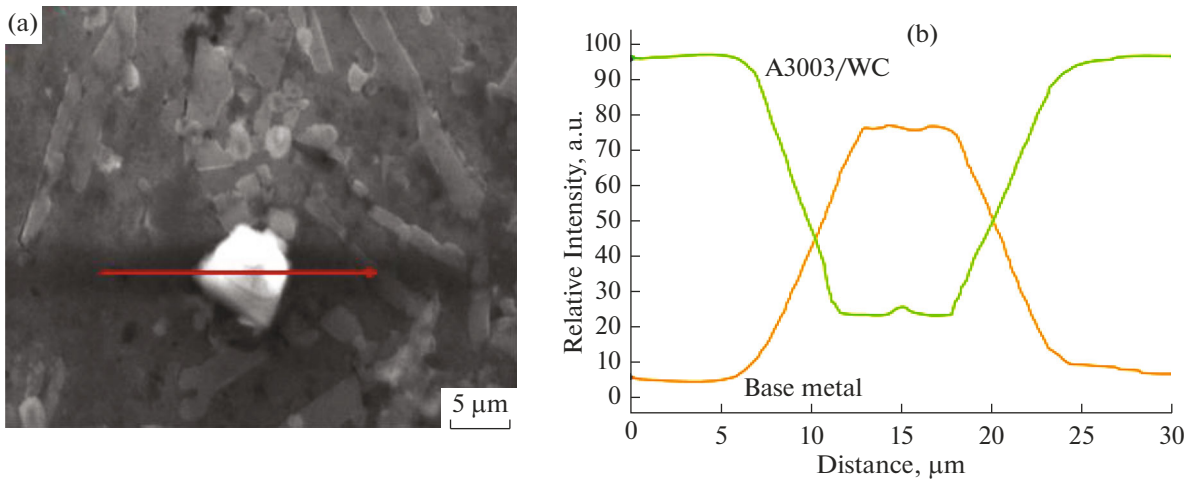

Fig. 6. Fabricated surface composite (A3003) interface of 6-pass FSP (a) FE-SEM image and (b) main elemental profiles in interface by EDXMA.

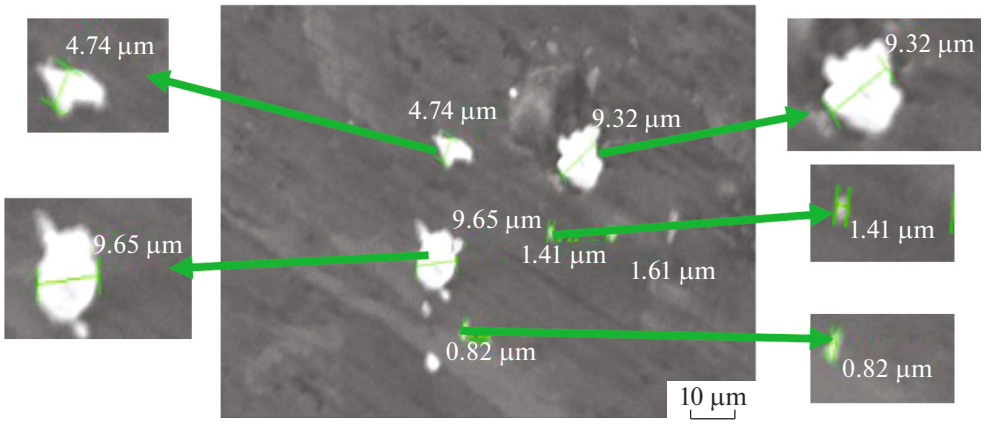

Fig. 7. FE-SEM micrograph after 6-pass friction stirred composite and grain refinement measurement.

change in the electronegativity of elements is contained by 0.5 [30–33]. The EDXMA image of the elemental profile of the base metal and as-modified surface composite (WC/A3003) are shown in Fig. 6b. The developed surface composite was experimentally predicted that the volume of the aluminum alloy (soft) element is larger than that of the WC particles (hard) diffused in the aluminum alloy matrix [34]. Specifically, the higher dispersion energy of WC arises from its extremely high melting point due to the higher dispersion percentage of aluminum alloy than tungsten carbide [35–37]. The FE-SEM images of the A3003 alloy and the WC-reinforced surface composite fabricated through multi-pass processed composite. The extruded microstructure with long, coarse grains in the cast alloying elements, microstructure of the 6-pass stirred composites and grains refinement shown in Fig. 7. Subsequently, compared to the alloy, upon adding WC particles, the grain size is reduced to 15 μm after 2 passes.

Due to plastic deformation and thermal effects increase the temperature of the materials in the stir zone via the rotating tool [38]. The FSP passes increases from 2 to 4 to 6, the grain-size in the stirred zone decreases from 5 to 1.5 to 1.2 μm, respectively. This observation moderately differs from the conclusions drawn from previous investigations stating that the FSP variables lead for uniform grains into Al-alloys matrix [39, 40]. Also, it was found that increasing of FSP passes decreases the amount of stirred WC, and the WC particles were circulated between matrix. The uniform distribution of the reinforcement particles allows for the fine-tuning of grains due to the sticking effect at the interface [41]. Secondly, the excellent spreading of WC microparticles reached after several processed passes increases with new nucleation locations and thus decreases the grains. Thirdly, individual FSP passes refine ounce but also develop the number of WC/A3003 interfaces due to good WC dispersion. Therefore, upon increasing the grain bound-

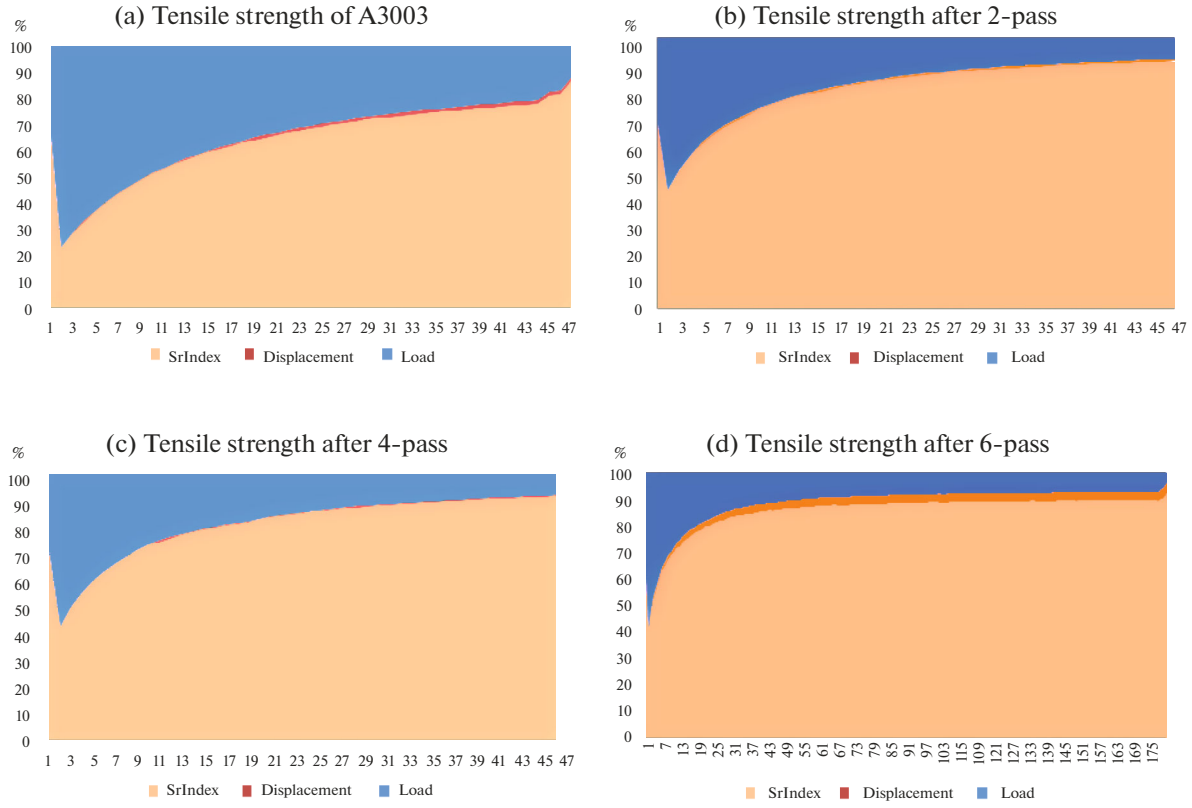

Fig. 8. Strain index of tensile test (a) base metal (A3003), and processed composite with different passes; (b) 2-pass; (c) 4-pass; (d) 6-pass.

aries of the WC/A3003 matrix, the enhanced interruption density increases the spontaneous formation of low angle sub-grains interfaces at the high stacking energy fault of A3003 for higher grain refinement into matrix.

However, there are no specious changes in grain size into stir zone of the aluminum alloy without WC particles. In the presence of WC particles in the stir zone, the particle size of the A3003 surface composite should decrease with increase of FSP passes.

3.3. Mechanical Characteristics

3.3.1. Tensile property. The specimens were subjected to the tensile test until fracture. The development of necking is apparent in the A3003 and 6-pass surface composite, as seen in Figs. 8a–8d, whereas there is no apparent mark on the necking of the 2-pass and 4-pass surface composites. Figure 9 shows the engineering stress-strain curves (in the stir zone) of the casted A3003 and the surface composites processed with multiple passes. The tensile strength of the processed composites is listed in Table 2. The ultimate tensile strength (UTS) at 0.2% proof stress increases with the number of FSP passes.

The enhanced tensile strength may be explained as follows. First, the tensile strength of A3003 increases with decrease in grain size due to the fine-grained strengthening (Hall–Patch equation). Dislocations will develop throughout the fine-grain structure during alloying owing to the different crystal orders of adjacent grains. Hence, the directions of crystal of the dislocations may change. Secondly, the development of geometrically (structural) essential dislocations could be delay [47], and the stress of the additional thermal expansion dislocation strengthens the WC

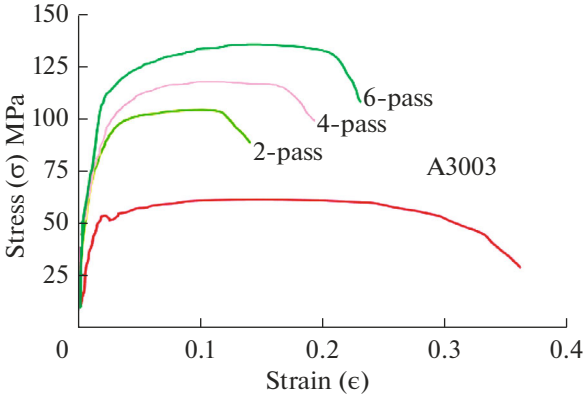

Fig. 9. S-N curves of A3003 and FSPed composite at various passes.

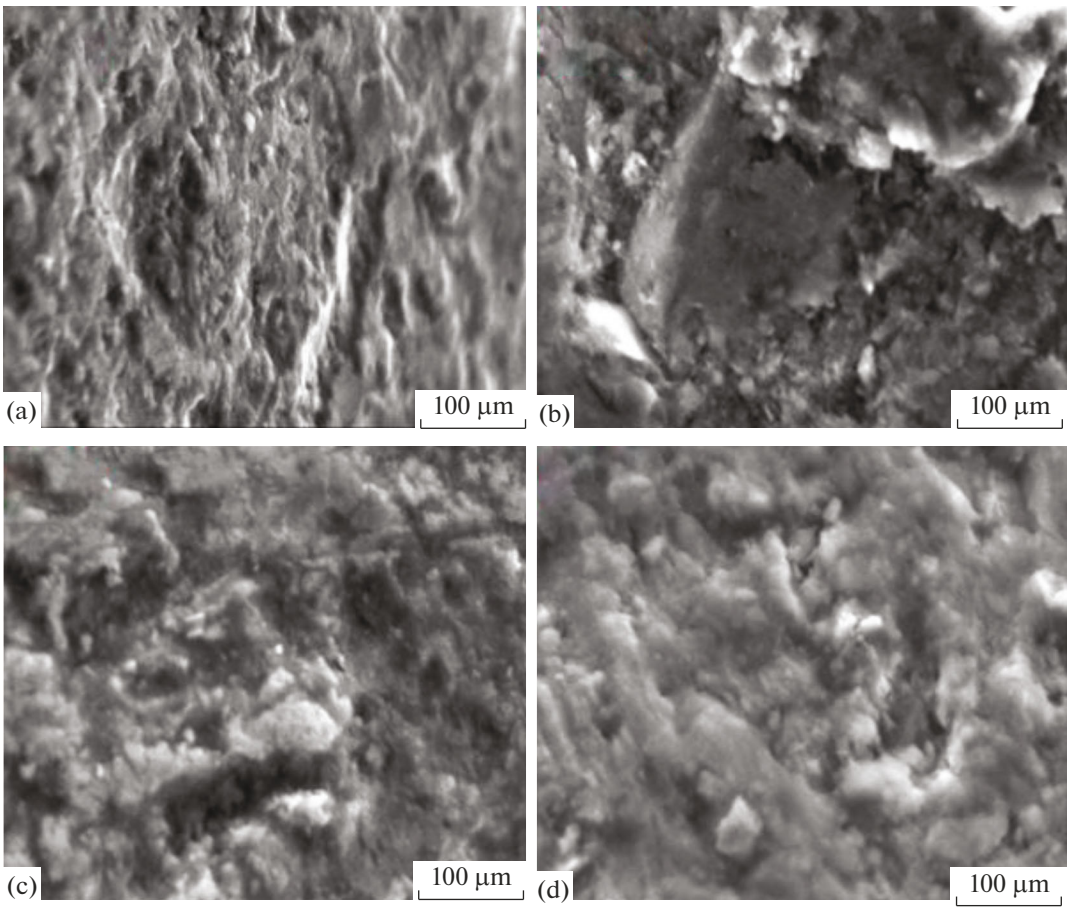

Fig. 10. Tensile fracto-graphs of (a) base metal (A3003) and FSPed composite (b) 2-pass; (c) 4-pass; (d) 6-pass at different passes.

grains. The geometrical dislocations are produced at the attached atoms interfaces owing to incompatibility for thermal expansion of the matrix and WC particles [49, 50]. Therefore, large variations in the thermal coefficient of the A3003 matrix (23.2×10^{-6}/°C) and WC particles (5.2×10^{-6}/°C) lead to the development of geometrical dislocations. The tungsten carbide particles are distributed more uniformly into the stir zone with increase in the number of FSP passes. Hence, the strength is also improved with increase in the number of FSP passes. Specifically, the strength of the matrix is improved via the reinforcing WC grains. Few significant properties such as ductility after compilations of 6-pass FSP (30%) at the same time reserved with aluminium cast-alloy (A3003; 35%).

Table 2. Tensile properties of the A3003 and FSP composites with different passes

Material	0.2% proof stress, MPa	UTS, MPa	Elongation, %
A3003	46.80	94.52	35.45
2-pass	74.79	116.83	14.51
4-pass	86.45	128.47	21.23
6-pass	91.50	143.10	30.15

This behaviour is different than that of a carbide-reinforced matrix, in which a markedly enhanced strength is associated with a strictly declining ductility. It was showed that an Al–4.5 Cu matrix reinforced with 5 vol% TiB_2 exhibited better yield stress (122 MPa) and only 6.5% elongation. Strong interfacial bonding of the A3003 matrix with the WC particles is achieved after 6 passes, as exposed in Fig. 5c. However, for smaller number of passes, the ductile elongation to rupture is considerably lower when the strength was improved. FE-SEM images of the tensile fracture of aluminum alloy (A3003) and composites processed with multi-passes are shown in Fig. 10. Deep pits and trim edges are witnessed on rupture surface of A3003 that designate typically ductile fissure that stops the nucleation mechanism of cracks as revealed in Fig. 10a. In addition, the same type of failure occurs after multiple passes, as shown in Figs. 10b–10d. However, the formed pits with WC particles specify the influence of WC particles on the flexibility of the disorders, confirming the excellent interfacial bonding into the developed matrix. Hence, the combination of good

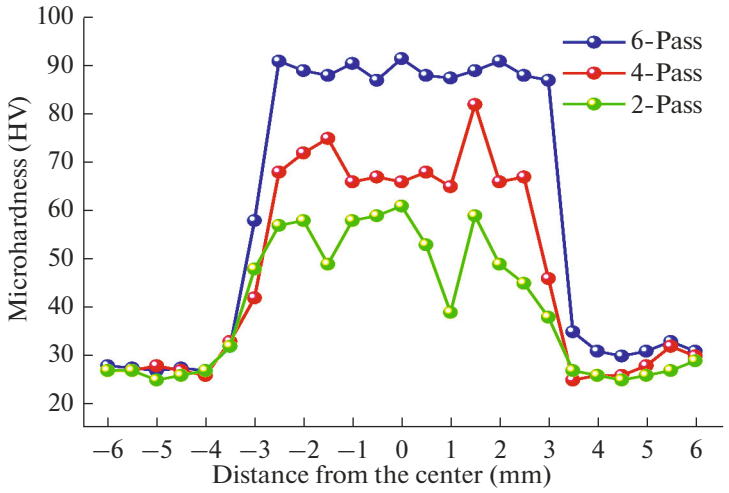

Fig. 11. Microhardness values of FSP composite at different passes (2, 4 and 6 pass).

ductility and higher strength is achieved in the 6-pass stirred surface.

3.3.2. Microhardness measurement. The observed microhardness of the processed surface is shown in Fig. 11. The hardness of the processed surface composites is higher than the cast aluminum alloy (~35 HV). The average microhardness of the developed composites increases with increase of FSP passes, reaching ~91.5 HV for the 6-pass FSP composite. The significant increased microhardness may be credited to (i) the WC distribution mechanism and (ii) the Hall–Petch consolidation mechanism due to ultra-fine grain of developed A3003/WC matrix. This results in the development of interruptions owing to thermal coefficient difference of WC particles and the new matrix. Furthermore, the increasing number of FSP passes leads to uniform distribution of microhardness, which may be ascribed to the excellent distribution of the WC particles with increases processing passes.

4. CONCLUSIONS

This research, a new developed surface composite (WC/A3003) was successfully fabricated through multi FSP passes. The microstructural, interfacial-bonding analysis and microhardness, and tensile behaviour of the developed composites as well as the effect of the various passes were summarised systematically. As the FSP passes increases dispersion of WC particles was improved, suggestively reducing the size of the tungsten carbide reinforcement particles in the matrix. As a result, several plastic deformations via fraternisation occurred because of the repeated thermal exposure and accumulated plastic strain. After 6-passes, the WC/A3003 composite does not contain tungsten oxide. The solid solution between the matrix and the grains with exceptional metallurgical bonding is entirely changed into fine grains with increase the FSP passes. A ductility (% elongation), tensile strength, and microhardness of 30%, 143 MPa, and 91.5 HV, respectively, were achieved after 6 passes. Consequently, the detailed description of the surface composite developed with multiple FSP passes provided interesting and useful outcomes for further applications.

REFERENCES

1. Tsao, L.C., Weng, W.P., Cheng, M.D., Tsao, C.W., and Chuang T.H., *J. Mater. Eng. Perform.,* 2011, vol. 11, p. 360.
2. Fujii, Hiromichi T., Sriraman, M.R., and Babu, S.S., *Metall. Mater. Trans. A,* 2011, vol. 42, p. 4045.
3. Seung I Cha, Soon H Hong, Gook H Ha, and Byung K Kim, *Scr. Mater.,* 2001, vol. 44, p. 1535.
4. Vedavyas, T., Arora, A., Gwalani, B., Mishra, R.S., Brennan, R.E., and Cho, K.C., *Mater. Sci. Eng., A,* 2018, vol. 709, p. 105.
5. Amirafshar, A. and Pouraliakbar, H., *Measurement,* 2015, vol. 68, p. 111.
6. Golmohammadi, M., Atapour, M., and Ashrafi, A., *Mater. Des.,* 2015, vol. 85, p. 471.
7. Barenji, R.V., Khojastehnezhad, V.M., Pourasl, H., and Rabiezadeh, A., *J. Compos. Mater.,* 2015, vol. 50, no. 11, p. 1457.
8. Akbari, M., Shojaeefard, M.H., Asadi, P., and Khalkhali, A., *J. Mater.: Des. Appl.,* 2017, vol. 233, no. 5, pp. 790–799. https://doi.org/10.1177/1464420717702413
9. Shojaeefard, M.H., Akbari, M., Khalkhali, A., and Asad, P., *J. Mater.: Des. Appl.,* 2016, vol. 232, no. 8, pp. 637–651. https://doi.org/10.1177/1464420716642471
10. Du, Z., Tan, M.-J., Guo, J.-F., and Wei, J., *J. Mater.: Des. Appl.,* 2016, vol. 230, no. 3, p. 825.
11. Ke, L., Huang, C., Xing, L., and Huang, K., *J. Alloys Compd.,* 2010, vol. 503, no. 3, p. 494.

12. Khalid, A., A-Ghamdi Hussain, G., and Hashemi, R., *J. Eng. Manuf.,* 2015, vol. 231, no. 8, p. 1319.
13. Sudhakar, I., Madhusudhan, R.G., and Srinivasa, R.K., *Def. Technol.,* 2016, vol. 12, no. 1, p. 25.
14. Selvakumar, S., Dinaharan, I., Palanivel, R., and Babu, B.G., *Mater. Charact.,* 2017, vol. 125, p. 13.
15. Kumar, S.S., Gopalakrishnan, S., Dinaharan, I., and Kalaiselvan, K., *Surf. Coat. Technol.,* 2017, vol. 322, p. 51.
16. Zeidabadi, S.R.H. and Daneshmanesh, H., *Mater. Sci. Eng., A,* 2017, vol. 702, p. 189.
17. Janbozorgi, M., Shamanian, M., Sadeghian, M., and Sepehrinia, P., *Trans. Nonferrous Met. Soc. China,* 2017, vol. 207, p. 298.
18. Kishan, V., Devaraju, A., and Lakshmi, K.P., *Def. Technol.,* 2016, vol. 13, no. 1, p. 16.
19. Heidarpour, A., Ahmadifard, S., and Kazemi Sh., *Prot. Met. Phys. Chem. Surf.,* 2018, vol. 54, p. 409.
20. Kamal, J.R., Malarvizhi, S., and Balasubramanian, V., *Def. Technol.,* 2017, vol. 13, no. 2, p. 111.
21. Akbari, M., Khalkhali, A., Keshavarz, S., Mohammad, E., and Ebrahim, S., *J. Mater.: Des. Appl.,* 2016, vol. 232, no. 5, pp. 429–437. https://doi.org/10.1177/1464420716630569
22. Ahmadifard, S., Kazemi, S., and Heidarpou, A., *J. Mater.: Des. Appl.,* 2015, vol. 232, no. 4, p. 287.
23. Akbari, M., Khalkhali, A., Keshavarz, S., Mohammad, S., and Ebrahim, E., *J. Mater.: Des. Appl.,* 2015, vol. 232, no. 3, pp. 213–229.
24. Abdollahi, S.H., Karimzadeh, F., and Enayati, M.H., *J. Alloys Compd.,* 2015, vol. 623, p. 335.
25. Eskandari, H. and Taheri, R., *Procedia Mater. Sci.,* 2015, vol. 11, p. 503.
26. Sree, S.S., Malarvizhi, S., Balasubramanian, V., and Madusudhan, R.G., *Def. Technol.,* 2016, vol. 12, no. 4, p. 324.
27. Vignesh, S., Shanmugam, K., Balasubramanian. V., and Sridhar, K., *Def. Technol.,* 2017, vol. 13, no. 2, p. 101.
28. Selvakumar, S., Dinaharan, I., Palanivel, R., and Babu, B.G., *Mater. Sci. Eng., A,* 2017, vol. 685, p. 317.
29. Likholobov, V.A., P'yanova, L.G., Boronin, A.I., Koshcheev, S.V., Salanov, A.N., Baklanova, O.N., Knyazheva, O.A., and Veselovskaya, A.V., *Prot. Met. Phys. Chem. Surf.,* 2011, vol. 47, p. 181.
30. Fayomi, O.S.I., Popoola, A.P.I., Loto, C.A., et al., *Prot. Met. Phys. Chem. Surf.,* 2016, vol. 52, p. 238.
31. Petrova, A., Brodova, I., Shorokhov, E., Plekhov, O., and Naimark, O., *Mater. Sci. Eng.,* 2014, vol. 63, p. 012146.
32. Zhang, H., Dong, X., and Chen, S., *Adv. Mech. Eng.,* 2017, vol. 9, p. 1.
33. Rathee, S., Maheshwari, S., Siddiquee, A.N., and Srivastava, M., *Def. Technol.,* 2017, vol. 13, p. 86.
34. Kokatev, A.N., Lukiyanchuk, I.V., Yakovleva, N.M., et al., *Prot. Met. Phys. Chem. Surf.,* 2016, vol. 52, p. 832.
35. Suresha, S. and Sridhara, B.K., *Compos. Sci. Technol.,* 2010, vol. 70, p. 1652.
36. Kotenev, V.A. and Vysotskii, V.V., *Prot. Met. Phys. Chem. Surf.,* 2019, vol. 55, p. 880.
37. Bolelli, G., Bonferroni, B., Laurila, J., Lusvarghi, L., Niemib, A., Milanti, K., and Vuoristo, P., *Wear,* 2012, vols. 276–277, pp. 29–47.
38. Mazahery, A. and Shabani, M.O., *Prot. Met. Phys. Chem. Surf.,* 2014, vol. 50, p. 817.
39. Chatha, S.S., Hazoor, S.S., and Buta, S.S., *J. Miner. Mater. Charact. Eng.,* 2012, vol. 11, p. 569.
40. Miguel, J.M., Guilemany, J.M., and Vizcaino, S., *Tribol. Int.,* 2003, vol. 36, p. 181.
41. Gao, Q., Wu, S., LÜ, S.D., and Xuecheng, A.P., *Mater. Des.,* 2016, vol. 94, p. 79.
42. Karabulut, Ş., Gökmen, U., and Çinici, H., *Composites, Part B,* 2016, vol. 93, p. 43.
43. Lotfi, N., Aliofkhazraei, M., Rahmani, H., et al., *Prot. Met. Phys. Chem. Surf.,* 2018, vol. 54, p. 1102.
44. Narimani, M., Lotfi, B., and Sadeghian, Z., *Surf. Coat. Technol.,* 2016, vol. 285, pp. 1–10.
45. Huang, G., Shen, Y., Guo, R., and Guan, W., *Mater. Sci. Eng., A,* 2016, vol. 674, p. 504.
46. Khamaj, J.A., *Prot. Met. Phys. Chem. Surf.,* 2016, vol. 52, p. 886.
47. Kokatev, A.N., Lukiyanchuk, I.V., Yakovleva, N.M., et al., *Prot. Met. Phys. Chem. Surf.,* 2016, vol. 52, p. 832.